Available online at www.sciencedirect.com
ScienceDirect
Journal of Nuclear Materials 361 (2007) 239–247
journal of nuclear materials
www.elsevier.com/locate/jnucmat

Dose dependence of true stress parameters in irradiated bcc, fcc, and hcp metals ☆

T.S. Byun *

Oak Ridge National Laboratory, P.O. Box 2008, MS-6151, Oak Ridge, TN 37831, USA

Abstract

The dose dependence of true stress parameters has been investigated for nuclear structural materials: A533B pressure vessel steels, modified 9Cr–1Mo and 9Cr–2WVTa ferritic martensitic steels, 316 and 316LN stainless steels, and Zircaloy-4. After irradiation to significant doses, these alloys show radiation-induced strengthening and often experience prompt necking at yield followed by large necking deformation. In the present work, the critical true stresses for deformation and fracture events, such as yield stress (YS), plastic instability stress (PIS), and true fracture stress (FS), were obtained from uniaxial tensile tests or calculated using a linear strain-hardening model for necking deformation. At low dose levels where no significant embrittlement was detected, the true fracture stress was nearly independent of dose. The plastic instability stress was also independent of dose before the critical dose-to-prompt-necking at yield was reached. A few bcc alloys such as ferritic martensitic steels experienced significant embrittlement at doses above ~1 dpa; and the true fracture stress decreased with dose. The materials fractured before yield at or above 10 dpa.

1. Introduction

Ductile metals experience an increase of strength and reduction of ductility after low temperature irradiation, which sometimes results in embrittlement [1–9]. In recent studies, the true stress–true strain behavior has been emphasized in the analysis of radiation effects to understand the correlation between microstructural evolution and mechanical properties [10–13]. In the past, the ductility loss by irradiation has been explained by a reduction in strain-hardening capability [1,8,9], resulting from a softening effect by dislocation channeling, where radiation-induced defects are cleared by glide of confined multiple dislocations [2,14–17]. In the analyses using true stress and true strain units, however, different descriptions of the radiation effects on strength and ductility have been suggested: the strain-hardening behavior at a given true stress level is not changed by irradiation [10–13,18,19]. This indicates that the strain-hardening portions of the true stress–true strain curves for irradiated iron can be superimposed on the curves for unirradiated material by shifting them in the positive direction along the strain axis [18]. A possible interpretation on radiation effects is that neutron irradiation has an effect similar to that of plastic deformation on the strain-hardening rate [11,12,19], regardless of

☆ This research was sponsored by US Department of Energy, Office of Fusion Energy Sciences, under Contract DE-AC05-00OR22725 with UT-Battelle, LLC.
* Tel.: +1 865 576 7738; fax: +1 865 574 0641.
E-mail address: byunts@ornl.gov

0022-3115/$ - see front matter © 2006 Elsevier B.V. All rights reserved.
doi:10.1016/j.jnucmat.2006.12.014

significant difference in detailed hardening mechanisms. This should also suggest that some true stress parameters should be dose-independent.

Recently, the author has extensively analyzed tensile test data for dozens of irradiated polycrystalline metals and developed theoretical models for localized deformation to correlate with strain hardening behaviors [11,12,20]. The results are summarized as: (1) the engineering tensile curve after low temperature neutron or proton irradiation showed necking at yield when the yield stress was above the plastic instability stress (PIS) of the unirradiated material; when the YS is below PIS, PIS is approximately independent of dose. (2) It was confirmed that two different defect structures, radiation-induced defects and deformation-produced dislocations, result in similar net effects on strain-hardening behavior [19]. (3) The dose independence of strain-hardening behavior was explained by a theoretical model for localized deformation: a strong back stress is generated in localized deformation, and consequently similar strain-hardening behaviors are produced by channel (or twinning) deformation in irradiated materials and by the uniform deformation in unirradiated materials [20].

The importance of unstable deformation after the onset of necking has been largely ignored in studying mechanical properties, although it may be a larger part of the whole deformation of a ductile material. In the present study, therefore, the true stress calculation is extended to the unstable (or necking) deformation of irradiated and unirradiated metallic materials. In this calculation, the true stress during unstable deformation was assumed to be a linear function of true strain, and the observation that the strain hardening rate after the onset of necking equals the plastic instability stress was used for constructing a strain hardening curve. Invariant volume was also assumed for plastic deformation [12,13]. The results indicated that the true fracture stress was nearly independent of dose before the material was embrittled. Mapping of deformation modes in the true stress-dose coordinates using the true stress parameters is presented.

2. Experiments and calculations

2.1. Irradiation experiments and tensile testing

Several dozen sets of tensile test data for irradiated materials have been produced in multiple research programs using sub-sized plate specimens: SS-3, S-1, and BES/NERI types [2,6–13,17]. Since this study focused on the radiation effects on true stress parameters including true fracture stress, only the experimental results which included fracture strength measurements were analyzed. Table 1 lists 12 irradiation experiments, which were designed to test key nuclear structural materials. Six bcc, fcc, and hcp metals were selected for this study: the bcc metals consisted of a pressure vessel steel (A533B) and two ferritic martensitic (FM) steels (9Cr–1MoVNb, 9Cr–2WVTa); the fcc metals selected were two austenitic stainless steels (316 and EC316LN); the hcp metal was Zircaloy-4 with two slightly different heat treatments. The chemical compositions and heat treatments for these alloys are given in Table 2.

Irradiation experiments were performed at two different facilities at nominal temperatures under 200 °C: the Hydraulic Tube facility of the High Flux Isotope Reactor (HFIR) at the Oak Ridge National Laboratory and the target area of the Los Alamos Neutron Scattering Center (LANSCE) accelerator at the Los Alamos National Laboratory. Irradiation conditions for tensile specimens are summarized in Table 1. In the HFIR irradiation facility, the tensile specimens were exposed to fast neutrons ($E > 0.1$ MeV) for different periods to achieve target damage levels. The irradiation temperature in the HFIR irradiation facility was estimated to be in the range 60–100 °C. In the LANSCE accelerator, the tensile specimens were irradiated at different target-area locations for different irradiation exposures to protons and spallation neutrons. The kinetic energy of the incident protons was 800 MeV and nuclear reactions by the protons produce spallation neutrons. The protons produced most of displacement damage in specimens at the front positions of the target ($p > n$ area) while the spallation neutrons made more or similar contributions to the damage at the back positions of the target ($n > p$ area). Total dose for each alloy (from protons and neutrons) is included in displacements per atom (dpa) data in Table 1. The maximum temperature measured by thermocouples was in the range 50–260 °C during irradiation [21].

All tensile tests were conducted at room temperature in screw-driven machines at crosshead speeds of 0.008 mm s^{-1} for SS-3 and BES/NERI type samples, and 0.005 mm s^{-1} for S-1 type specimens; both speeds correspond to a strain rate of about 10^{-3} s^{-1}. The load–displacement curves were recorded and used to

Table 1
Summary of irradiation experiments

Case #	Material	Specimen type[a]	Irradiation facility	Dose range (dpa)	Irradiation temperature (°C)
1	A533B	BES/NERI	HFIR (n)[b]	0–0.89	60–100
2	A533B	SS-3	HFIR (n)	0–1.28	60–100
3	9Cr–2WVTa	S-1	LANSCE ($n < p$)	0–10.15	50–160
4	9Cr–2WVTa	SS-3	LANSCE ($n > p$)	0–0.12	90–260
5	9Cr–1MoVNb	S-1	LANSCE ($n < p$)	0–10.15	50–160
6	9Cr–1MoVNb	SS-3	LANSCE ($n > p$)	0–0.12	90–260
7	316	BES/NERI	HFIR (n)	0–0.78	60–100
8	EC316LN	S-1	LANSCE ($n < p$)	0–10.67	50–160
9	EC316LN	SS-3	LANSCE ($n > p$)	0 – 0.12	90–260
10	Zr-4	BES/NERI	HFIR (n)	0–0.8	60–100
11	Zr-4	S-1	LANSCE ($n < p$)	0–24.58	50–160
12	Zr-4	SS-3	LANSCE ($n > p$)	0–0.12	90–260

[a] Gage section dimensions for SS-3, S-1, and BES/NERI types are $0.76 \times 1.52 \times 7.62$, $0.25 \times 1.2 \times 5$, and $0.25 \times 1.5 \times 8$ mm^3, respectively.
[b] Irradiation particles: (n) – fast neutron irradiation; ($n < p$) – high energy proton dominant in the mixture of incident protons and spallation neutrons; ($n > p$) – fast neutron dominant in the mixture of incident protons and spallation neutrons.

Table 2
Materials and heat treatments for bcc, fcc, and hcp metals

Case #	Material	Crystal	Chemical composition (wt%)	Heat treatment (in vacuum unless specified)
1	A533B	bcc	Fe–0.22C–0.25Si–1.48Mn–0.52Mo–0.68Ni–0.018S–0.012P	Annealed at 880 °C for 4 h and air cooled, tempered at 660 °C for 4 h, reheated at 610 °C for 20 h
2				
3	9Cr–2WVTa (Low activation steel)	bcc	Fe–0.11C–0.44Mn–0.21Si–0.015P–8.9Cr–0.01Mo–0.23V–0.012Co–0.03Cu–0.017Al–2.01W–0.06Ta	Heated for 1 h at 1050 °C in flowing argon and cooled; then reheated for 1 h at 750 °C and cooled
4				
5	9Cr–1MoVNb (Modified 9Cr–1Mo steel)	bcc	Fe–0.092C–0.09Ni–8.32Cr–0.86Mo–0.48Mn–0.15Si–0.055N–0.06Nb–0.2V	Heated for 1 h at 1050 °C in flowing argon and cooled; then reheated for 1 h at 750 °C and cooled
6				
7	316	fcc	Fe–0.059C–1.86Mn–0.57Si–0.018S–0.024P–17.15Cr–13.45Ni–2.34Mo–0.1Cu–0. 02Co–0.031N	Annealed at 1050 °C for 30 min
8	EC316LN	fcc	Fe–12.2Ni–17.45Cr–2.5Mo–1.81Mn–0.39Si–0.024C–0.067N	Annealed at 950 °C for 1 h
9				
10	Zr-4	hcp	Zr–1.4Sn–0.015C–0.1Fe–0.001S–0.06O–<0.1Ni–<0.001N	Annealed at 670 °C for 30 min
11	Zr-4	hcp	Zr–1.4Sn–0.015C–0.1Fe–0.001S–0.06O–<0.1Ni–<0.001N	Annealed at 710 °C for 30 min
12				

calculate true stress parameters. The constant volume condition [22] was used for the calculation of plastic strain components throughout this study.

2.2. Calculations

In the development of deformation mode maps in true stress-dose space, the yield stress, plastic instability stress, and fracture stress are needed as the boundaries between deformation modes. The yield stress and plastic instability stress are obtained from the engineering tensile data while the fracture stress and strain are calculated using a method described below. This calculation method is based on a linear strain hardening model for necking deformation [13]. Assuming linear true stress–true

strain curves for necking deformation, the values for average strain-hardening rate during necking (HRN) were empirically evaluated for the annealed 316LN, 20% cold-worked 316LN, annealed 304, and annealed and irradiated 304 stainless steels, and they were compared with their plastic instability stress values [7,13,14]. The comparisons revealed that the magnitude and temperature dependence of HRN were approximately the same as those of the plastic instability stress above room temperature, where no martensitic transformation occurred. It has been confirmed that the strain-hardening rate is positive during necking in both irradiated and unirradiated materials although the engineering stress decreases with elongation [18–20]. This should be valid as long as there is a diffuse neck, which occurs usually in ductile metals before a final failure by localized shear (banding) or cleavage initiation. The finding that the strain-hardening rate remains nearly unchanged at plastic instability stress during necking leads to the use of linear true stress–true strain curves for necking deformation. Such high, constant HRN values during necking were explained by a balance between two effects: (1) the decreasing load carrying capability due to contraction of the cross-sectional area and due to reduction in the hardening rate in the equivalent stress–strain response and (2) the increasing constraint effect from increasing stress triaxiality in the neck.

With constant strain-hardening rates during necking, a true stress–true strain curve during necking ($\varepsilon_U \leqslant \varepsilon \leqslant \varepsilon_F$) can be expressed by a linear equation [13]

$$\sigma(\varepsilon) = \max(\sigma_{YS}, \sigma_{PI}) + \sigma_{PI}(\varepsilon - \varepsilon_U), \quad (1)$$

where ε_U, ε_F, σ_{YS} and σ_{PI} are the true uniform strain, the fracture strain, the yield stress and the plastic instability stress (PIS), respectively. The slope of curve or plastic instability stress can be calculated from the UTS using the constant volume condition during plastic deformation

$$\sigma_{PI} = \mathrm{UTS} \times \exp(\varepsilon_U). \quad (2)$$

Then, the true fracture stress σ_F can be calculated by replacing ε with ε_F in Eq. (1)

$$\sigma_F = \max(\sigma_{YS}, \sigma_{PI}) + \sigma_{PI}(\varepsilon_F - \varepsilon_U), \quad (3)$$

or from the engineering fracture strength (EFS) using the constant volume condition

$$\sigma_F = \mathrm{EFS} \times \exp(\varepsilon_F). \quad (4)$$

The solution for ε_f and σ_F can be obtained by iterative calculation using Eqs. (3) and (4) and engineering tensile data.

3. Results and discussion

3.1. Dose dependence of true stress parameters

Figs. 1 and 2 present the dose dependencies of true stresses for steels (bcc). In the A533B steel after low temperature neutron irradiation up to 1.3 dpa, the true fracture stress is nearly independent of dose with a large scatter. Moreover, the plastic instability stress is almost constant with smaller scatter [11]. Typically in thermally stabilized materials, the yield stress after low temperature irradiation is strongly dependent on dose [11]. For 9Cr–1MoVNb and 9Cr–2WVTa FM steels, the true stress data after irradiation in spallation conditions to higher doses are presented in Fig. 2. The true fracture stress varies within a range over a dose range of 0–1 dpa, while it decreases with dose above about 1 dpa until it experiences total embrittlement at 10.2 dpa. This indicates that the materials have been partially embrittled between 1 and 10.2 dpa.

Figs. 1 and 2 also depict the regions for macroscopic deformation modes such as the elastic deformation, uniform plastic deformation, and unstable (necking) deformation; the regions of these modes are defined by the true stress parameters. Comparing the sizes of the regions for deformation modes,

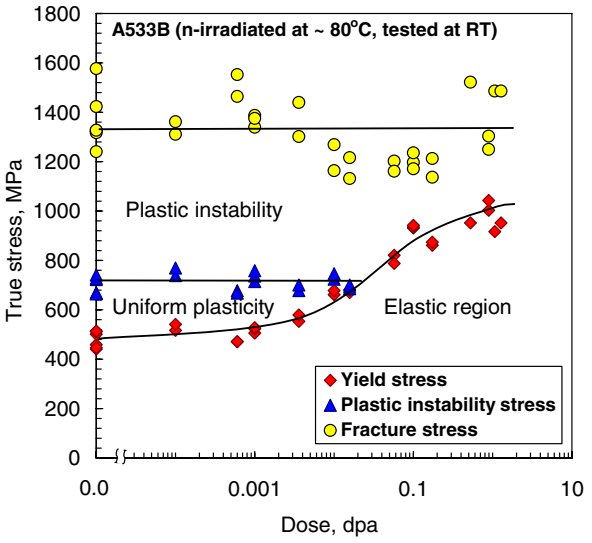

Fig. 1. Dose dependence of true stress parameters in A533B pressure vessel steel after low temperature neutron irradiation.

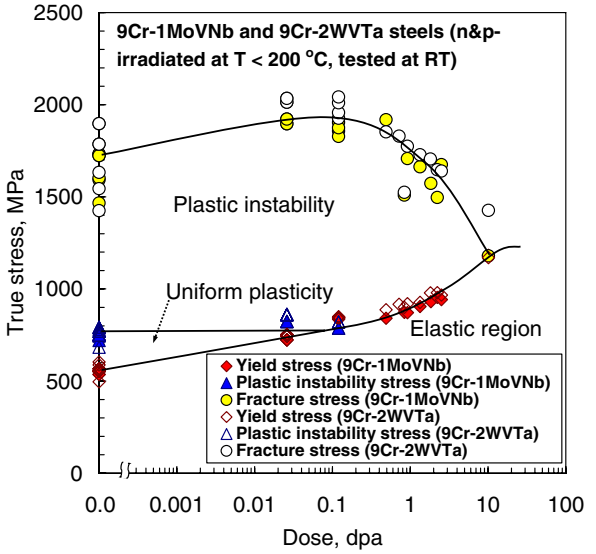

Fig. 2. Dose dependence of true stress parameters in ferritic martensitic steels after irradiation by high energy protons and spallation neutrons.

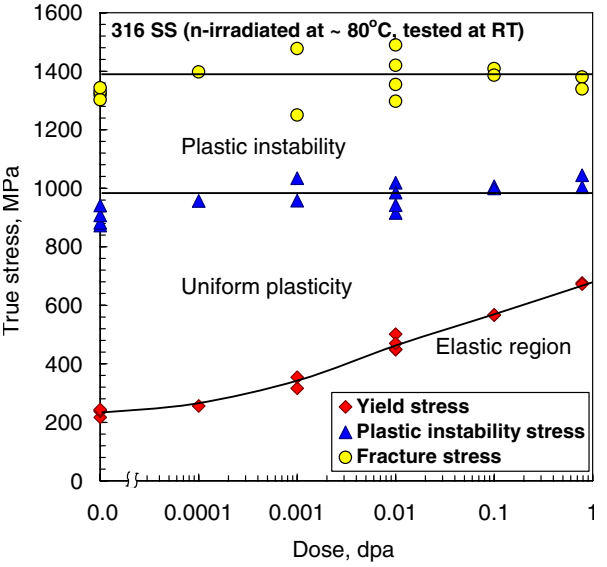

Fig. 3. Dose dependence of true stress parameters in 316 stainless steel after low temperature neutron irradiation.

the mode maps for bcc metals are characterized by a relatively large plastic instability region and a narrow uniform deformation region, which are due to large necking ductility and low strain-hardening rate, respectively. Such large plastic instability regions indicate that these quenched and tempered steels can retain significant fracture toughness up to ~1 dpa due to the instable deformation capability [8,23].

Figs. 3 and 4 present the macroscopic deformation mode maps for 316 and 316LN austenitic stainless steels. Again, the plastic instability stress and fracture stress are nearly independent of dose. In the fcc maps, the uniform deformation regions are relatively large when compared to the plastic instability regions. In these fcc metals the yield stresses are 200–300 MPa before irradiation and the plastic instability stresses are in the range 900–1000 MPa; the span between these stresses is wide, about 700 MPa before irradiation, Figs. 3 and 4. The span between the two stresses is smaller in bcc metals; about 200 MPa, as seen in Figs. 1 and 2. This large uniform deformation region delays the prompt necking at yield: In the 316 and 316LN stainless steels the yield stress increases with dose to above plastic instability stress at about 30 dpa, while in the A533B and FM steels the yield stress becomes higher than the plastic instability stress between 0.01 and 0.1 dpa. These differences between bcc and fcc metals agree with the fact that the strain-

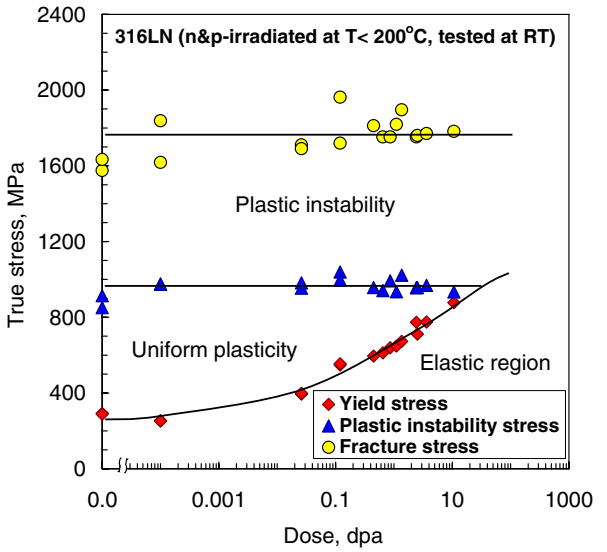

Fig. 4. Dose dependence of true stress parameters in 316LN stainless steel after irradiation by high energy protons and spallation neutrons.

hardening rate in fcc metals are generally higher than those in bcc metals, especially in high strain region.

The dose dependence of true stress parameters for a hcp metal (Zircaloy-4) is presented in Fig. 5. Here, the true fracture stress has a small dose-dependence; while the plastic instability does not show any dose dependence. It is found that the yield stress is far below the fracture stress at the highest dose, 24.5

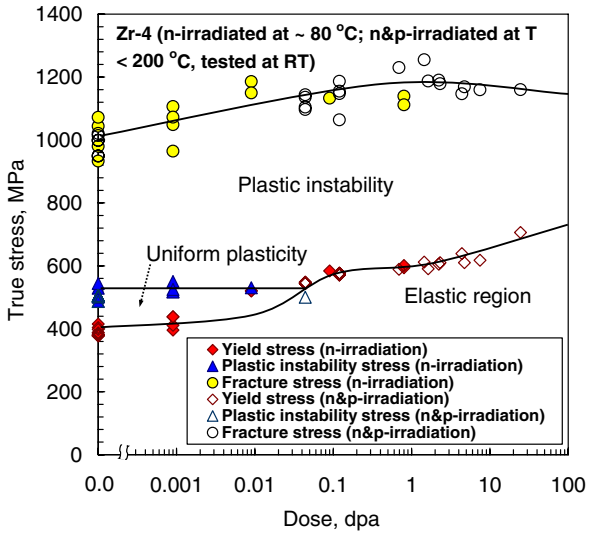

Fig. 5. Dose dependence of true stresses in Zircaloy-4 after irradiation by fast neutrons or by high energy protons and spallation neutrons.

dpa; which suggests that Zircaloy-4 experience embrittlement at very high doses such as above 100 dpa if the fracture stress does not decrease. Also, it is noted that the deformation mode map for Zircaloy-4 is similar to those of bcc metals.

3.2. Strain-hardening behavior and fracture stress

So far, most of the studies on strain-hardening behavior have been focused on stable or uniform deformation [1,23]. In the explanation of fracture behavior, however, the unstable deformation during necking might be as important as the uniform deformation since mechanical property like fracture toughness might be related to the fracture strain (and stress), and significant true necking strains are often measured in the irradiated specimens which experience necking at yield (or nil uniform ductility). The significance of unstable deformation is presented in the macroscopic deformation mode maps for bcc and hcp metals, Figs. 1, 2 and 5, where the unstable deformation region is much larger than the uniform deformation region. Also, it is found that the critical dose to prompt necking at yield (the dose at which the yield stress is above the plastic instability stress) is relatively low, between 0.01 and 0.1 dpa, in those bcc and hcp metals. The phenomenon occurs at a much higher dose of ~30 dpa in 316LN stainless steel where the uniform deformation region is relatively larger (see Fig. 4). Above the critical dose, only unstable deformation exists and controls the performance of the material until the material is totally embrittled either by a decrease of fracture stress, as seen in Fig. 2, or by an increase of yield stress.

It has been widely accepted that the loss of uniform ductility after irradiation, prior to necking, is related to the reduction of strain-hardening rate or to the softening effect due to the clearance of radiation-induced defects by glide dislocations [13–17,23–30]. This may be a possible explanation for the loss of ductility when the strain-hardening behaviors are compared at an equal 'strain' level or in engineering stress units. However, it was shown that the uniform ductility can be reduced by simply increasing the yield stress and/or by decreasing the strain hardening rate [9]. Indeed, experimental results indicated evidence of dose independent strain-hardening behavior. Mogford and Hull [19] and Ohr [18] found that the strain-hardening portions of the flow curves for a bcc material after irradiation to various doses were very similar if compared at the same 'stress' level, and therefore that they can be superimposed on the curve for unirradiated material by shifts along the strain axis. DiMelfi et al.'s results [31] confirmed the dose independence of strain-hardening behavior in neutron-irradiated iron-based alloys. The validity of this suggestion was tested by applying the shifting operation to A533B, EC316LN, and Zircaloy-4 alloys, as representative materials for bcc, fcc, and hcp crystal structures, respectively [11]. The results confirmed the invariance of strain-hardening rate after irradiation. On the superimposed portions, the strain-hardening rates of the irradiated specimens were nearly the same as those of the unirradiated material; the flow curve after irradiation represents part of the curve for the unirradiated material (see Fig. 6). It was also noted that the plastic instability stresses were comparable for all specimens when the strain shifts were adopted. The dose independence of the plastic instability stress was confirmed for at least two dozen polycrystalline metals [11].

These observations confirm that the radiation-induced defects do not significantly change the strain-hardening behavior of the material, and also confirm Mogford and Hull's suggestion [19] that there is an analogy between neutron irradiation and plastic deformation. It was also suggested that the dislocation–dislocation interactions and dislocation–defect cluster interactions produced similar net hardening effects at the same stress level [11]. Therefore, the final conclusion drawn from the invariance

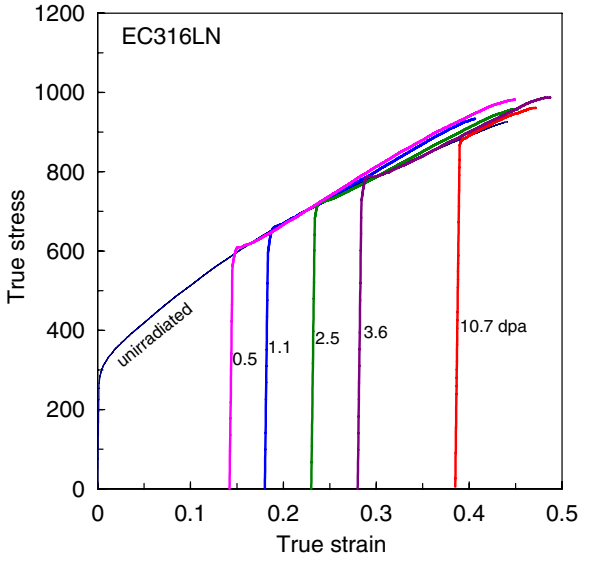

Fig. 6. True stress–true strain curves for EC316LN stainless steel; the curves of irradiated specimens are shifted in the positive direction by strains of 0.14, 0.18, 0.23, 0.28, and 0.385, respectively, to superimpose on the curve of unirradiated material. Irradiation-induced increases in yield stress were 305, 358, 421, 485, and 587 MPa, respectively [11].

of strain-hardening behavior is that the fracture should be nearly independent of irradiation dose, if no embrittlement mechanism exists. This agrees with what we observe in the mode maps in Figs. 1–5.

Previous studies [11,32] also indicate that the strain-hardening rate is not affected by the change in deformation mechanism from dislocation tangling to dislocation channeling induced by irradiation. An apparently reduced strain-hardening rate is displayed by the true stress–true strain curve of irradiated material because the flow curve corresponds to the high-strain portion of the curve for unirradiated material, which has a reduced strain-hardening rate. To explain the dose independence of strain-hardening behavior, two possible reasons were suggested [11]: (1) Similar true strain-hardening behaviors can be produced by the channel deformation in irradiated materials and by the uniform deformation in unirradiated materials. (2) Deformations in irradiated materials and in heavily-deformed unirradiated materials are both equally localized. If the first suggestion is correct, the strain-hardening rate due to the long-range back stresses in the channels in irradiated metals should be as high as that in the region of uniform deformation in unirradiated metals. Although the detailed mechanism of channel formation is largely unknown, a number of studies have confirmed that defect clusters are cleared within the channels [13–17,23–30]. A significant drop of local shear stress in the channel should occur because of this clearance in the early stage of channel formation; however, the local stress should return quickly to a stress level as high as those in adjacent regions as the back stress builds up [13,20,26].

A theoretical model for long-range back stress hardening was proposed to explain the strain-hardening behavior during strain localization [20]. In the modeling the long-range back stress was formulated as a function of the number of residual pileup dislocations at a grain boundary and the number of localized bands formed in a grain. The strain-hardening rates in channel deformation were calculated for face-centered cubic (fcc) and body-centered cubic (bcc) polycrystalline metals. It turned out that a few residual dislocations at each channel-grain boundary intercept could account for the strain-hardening rates as high as those for the uniform deformation by dislocation tangling. It was also shown that the strain-hardening behavior predicted by the long-range back stress model resembled the empirical strain-hardening behaviors which result from both localized and non-localized deformations. The plastic instability stress predicted for channeling was comparable to the tensile test data which resulted from all sorts of mechanisms such as dislocation tangling, channeling, and twinning. These results, therefore, indicated that at least the first term (1) in above suggestions is valid; the strain localization is not accompanied by significant change in macroscopic mechanical property or strain-hardening behavior, except for the increase of yield stress, which often comes with a yield drop.

3.3. The ratio of fracture stress to plastic instability stress

Since the plastic instability stress and true fracture stress represent the initiation and finish of necking deformation and the strain-hardening rate during the unstable deformation is nearly independent of dose if no embrittlement occurs, a relationship is expected to exist between those true stresses. Table 3 includes the average values of PIS and FS as well as their ratios (FS/PIS). The values of the stress ratio FS/PIS for A533B and 9Cr steels ranged from 1.8 to 2.4, while those for austenitic stainless steels are slightly lower; 1.4–1.9. The stress ratios for Zirca-

Table 3
Summary of true stress data

Case #	Material	Dose range[a], dpa	YS (0 a/highest dose) (MPa)	Average PIS[b] (MPa)	Average FS[c] (MPa)	FS/PIS
1	A533B	0–0.89	497/1023	732	1292	1.8
2	A533B	0–1.28	444/952	680	1348	2.0
3[a]	9Cr–2WVTa	0–10.15	562/1170	786	1741	2.2
4	9Cr–2WVTa	0–0.12	561/846	821	1964	2.4
5[a]	9Cr–1MoVNb	0–10.15	552/1183	767	1698	2.2
6	9Cr–1MoVNb	0–0.12	544/839	788	1842	2.3
7	316	0–0.78	234/674	975	1367	1.4
8	EC316LN	0–10.67	290/877	948	1755	1.9
9	EC316LN	0–0.12	253/551	987	1757	1.8
10	Zr-4	0–0.8	396/598	524	1072	2.0
11	Zr-4	0–24.58	386/706	500	1131	2.3
12	Zr-4	0–0.12	380/574	504	1069	2.1

[a] The whole dose range where specimens were tested.
[b] Average PIS for the cases with non-zero uniform ductility.
[c] Average FS for ductile failure only.

loy-4 are similar to those of A533B and 9Cr steels. These results indicate that the two true stress parameters have a strong relationship and represent the characteristics for each crystal type. Among the three crystal structures the fcc metals showed a relatively larger uniform deformation region, which should be due to higher strain-hardening capability. However, the fcc metals have relatively lower stress ratios.

The strong relationship between the two true stress parameters makes it possible to predict true fracture stresses from the plastic instability stress data. This may raise questions about the origin of the strong relationship between the onset of plastic instability and the final fracture, considering that the onset of necking occurs well before the fracture event. It is believed that with a significant plasticity the two critical stresses (plastic instability stress and fracture stress) are properties of the matrix. If this is the case, those stress parameters will not be affected by irradiation or introduction of other defects; as far as the volume of radiation-induced defects is negligible (less than a few percent for most irradiated materials), both unirradiated and irradiated materials have the same matrix, and consequently the same plastic instability stress and fracture stress. A change of matrix property, i.e., any significant change in alloy element distribution or in constituent phases, may result in changes of those true stress parameters.

4. Summary and conclusions

(1) The dose dependence of true stress parameters was investigated for polycrystalline metals after irradiation at low nominal temperatures (<200 °C). The macroscopic deformation modes such as elastic, stable and unstable plastic deformations were expressed in the maps on true stress vs. dose coordinates using the true stress parameters as boundaries.
(2) The plastic instability stress was nearly independent of dose below the critical dose for prompt necking at yield, above which the yield stress was higher than the plastic instability stress.
(3) The true fracture stress was also nearly independent of dose with significant scatter before embrittlement occurred. It was found that the fracture stress decreased with dose when an embrittlement mechanism operated.
(4) It is believed that the plastic instability stress and true fracture stress are material constants for a matrix in plastic deformation. Since the strain hardening due to long-range back stress in localized deformation can take over the hardening amount due to the dislocation tangling in uniform deformation, no significant radiation effect exists in strain-hardening behavior. It is apparent that there is a strong relationship between those two true stress parameters.

Acknowledgements

This research was sponsored by US Department of Energy, Offices of Fusion Energy Sciences and Basic Energy Science, under Contract DE-AC05-00OR22725 with UT-Battelle, LLC. The author

expresses special thanks to Drs J. Busby and M. Li for technical reviews and comments.

References

[1] J.E. Pawel, A.F. Rowcliffe, D.J. Alexander, M.L. Grossbeck, K. Shiba, J. Nucl. Mater. 202 (1996) 233.
[2] K. Farrell, T.S. Byun, J. Nucl. Mater. 296 (2001) 129.
[3] Y. Kitsunai, H. Kurishita, T. Kuwabara, M. Narui, M. Hasegawa, T. Takida, K. Takebe, J. Nucl. Mater. 346 (2005) 233.
[4] B.V. Cockeram, R.W. Smith, L.L. Snead, J. Nucl. Mater. 346 (2005) 145.
[5] B.V. Cockeram, R.W. Smith, L.L. Snead, J. Nucl. Mater. 346 (2005) 165.
[6] T.S. Byun, K. Farrell, E.H. Lee, J.D. Hunn, L.K. Mansur, J. Nucl. Mater. 298 (2001) 269.
[7] T.S. Byun, K. Farrell, E.H. Lee, L.K. Mansur, S.A. Maloy, M.R. James, W.R. Johnson, J. Nucl. Mater. 303 (2002) 34.
[8] K. Farrell, T.S. Byun, J. Nucl. Mater. 318 (2003) 274.
[9] T.S. Byun, K. Farrell, J. Nucl. Mater. 318 (2003) 292.
[10] T.S. Byun, K. Farrell, J. Nucl. Mater. 326 (2004) 86.
[11] T.S. Byun, K. Farrell, Acta Mater. 52 (2004) 1597.
[12] T.S. Byun, N. Hashimoto, K. Farrell, Acta Mater. 52 (2004) 3889.
[13] T.S. Byun, N. Hashimoto, K. Farrell, J. Nucl. Mater. 351 (2006) 303.
[14] M.S. Wechsler, in: The Inhomogeneity of Plastic Deformation, Am. Soc. for Metals, Metals Park, OH, 1971, Chapter 2.
[15] A. Luft, Progr. Mater. Sci. 35 (1991) 97.
[16] F.A. Smidt Jr., Dislocation Channeling in Irradiated Metals, NRL Report 7078, Naval Res. Lab., Washington DC, 1970.
[17] K. Farrell, T.S. Byun, N. Hashimoto, J. Nucl. Mater. 335 (2004) 471.
[18] S.M. Ohr, Scripta Metall. 2 (1968) 213.
[19] I.L. Mogford, D.J. Hull, Iron Steel Inst. 201 (1963) 55.
[20] T.S. Byun, N. Hashimoto, J. Nucl. Mater. 354 (2006) 123.
[21] S.A. Maloy, M.R. James, G. Willcutt, W.F. Sommer, M. Sokolov, L.L. Snead, M.L. Hamilton, F. Garner, J. Nucl. Mater. 296 (2001) 119.
[22] M.A. Meyers, K.K. Chawla, Mechanical Behavior of Materials, Prentice-Hall, 1998.
[23] G.R. Odette, M.Y. He, E.G. Donahue, G.E. Lucas, ASTM STP 1418 (2002) 221.
[24] J.V. Sharp, Acta Metal. 22 (1974) 449.
[25] J.V. Sharp, Philos. Mag. 16 (1967) 77.
[26] M.J. Makin, J.V. Sharp, Phys. Stat. Sol. 9 (1965) 109.
[27] R.P. Tucker, M.S. Wechsler, S.M. Ohr, J. Appl. Phys. 40 (1969) 400.
[28] S.J. Zinkle, B.N. Singh, Microstructure of neutron-irradiated iron before and after tensile deformation, J. Nucl. Mater. 351 (2006) 269.
[29] E.J. Edwards, B.N. Singh, J.B. Bilde-Sørensen, J. Nucl. Mater. 342 (2005) 164.
[30] T.S. Byun, N. Hashimoto, K. Farrell, E.H. Lee, J. Nucl. Mater. 349 (2006) 251.
[31] R.J. DiMelfi, D.E. Alexander, L.E. Rehn, J. Nucl. Mater. 252 (1998) 171.
[32] E.V. Van Osch, M.I. DeVries, J. Nucl. Mater. 271&272 (1991) 162.